Multiscale Measurements of Ocean Wave Breaking Probability

MICHAEL L. BANNER

School of Mathematics, The University of New South Wales, Sydney, New South Wales, Australia

JOHANNES R. GEMMRICH AND DAVID M. FARMER*

Institute of Ocean Sciences, Sidney, British Columbia, Canada

(Manuscript received 29 October 2001, in final form 7 May 2002)

ABSTRACT

Recent numerical model studies of nonlinear deep water wave group evolution suggest that wave breaking onset is associated primarily with a threshold behavior linked to the nonlinear wave group hydrodynamics. Motivated by these findings, a recently published probability analysis of observed dominant ocean wind wave breaking events reported a threshold behavior using the significant wave steepness as a measure of the mean nonlinearity of these waves. The present study investigates whether a similar threshold dependence in terms of an appropriate spectral measure of wave steepness, the spectral saturation, may be found for the breaking probability of shorter wind waves above the spectral peak. Extensive data records of open ocean whitecap breaking wave occurrences for wind speeds up to 18 m s^{-1} were analyzed for breaking probability dependence on spectral saturation in spectral bands with center frequencies ranging from 1 to 2.48 times the spectral peak frequency. Results are based on the measured ratio of passage rates past a fixed point of breaking crests to total crests for different wave scales. An extension of the zero-crossing method for counting wave crests was developed. Using this method the authors found that in any spectral subrange within the observed range of frequencies, a strong correlation exists between breaking probability and an appropriate mean spectral steepness parameter and that this correlation is characterized by a robust threshold behavior, just as was reported previously for the spectral peak waves. Further, to offset the influence of increasing directional spreading of the waves above the spectral peak frequency, an empirical directional spreading function was used to normalize the azimuth-integrated spectral saturation. Under this normalization, the spectral saturation threshold for breaking onset appears to have a common level over the frequency range investigated. This study also examined the correlation of breaking probability with spectral peak wave age. The low correlation found for all spectral ranges investigated suggests that nonlinear wave hydrodynamics are more important than wind forcing for the breaking of these wind waves.

1. Introduction

Breaking waves appearing in the form of whitecaps represent a very familiar yet poorly understood feature of the wind-driven sea surface. Especially when they occur as large-scale breakers, these waves represent the most hazardous conditions for seafarers and offshore structures. There is also an outstanding need for a more physically based dissipation source function in spectral wind wave models. Recent review articles by Banner and Peregrine (1993), Thorpe (1995), Melville (1996), and Duncan (2001) provide comprehensive overviews of the importance and scientific status of the major aspects of wave breaking and its importance for upper ocean dynamics and offshore engineering.

Recent efforts to provide a more complete understanding of breaking onset have been guided by numerical model studies of nonlinear wave groups (e.g., Dold and Peregrine 1986; Tulin and Li 1992; Banner and Tian 1998; Song and Banner 2002; Banner and Song 2002; among others). These studies suggest that the nonlinearity of dominant ocean waves underlies their modulational properties and has a major role in determining the onset of breaking. Laboratory wave tank studies by Rapp and Melville (1990), Tulin and Waseda (1999), and Waseda and Tulin (1999), among many others, have also contributed significant insight into the processes associated with wave breaking, especially in the postbreaking phase inaccessible to the irrotational wave model studies. Recent interest in this area has extended to laboratory observations of three-dimensional breaking waves (e.g., She et al. 1997; Nepf et al. 1998) but further research is needed to determine the relative importance of spectral bandwidth and directionality in the

* Current affiliation: Graduate School of Oceanography, University of Rhode Island, Narragansett, Rhode Island.

Corresponding author address: Prof. Michael L. Banner, School of Mathematics, The University of New South Wales, Sydney 2052, Australia.
E-mail: m.banner@unsw.edu.au

TABLE 1. Summary of experimental conditions, giving deployment number, location and date, wind direction dd, wind speed u_{10} corrected to 10-m height, significant wave height H_s, period of dominant wind waves τ_p, and nominal depth of shallowest conductivity sensor z_s. Standard deviations (σ) are given for wind direction and wind speed.

Expt	Date	Location	Fetch (km)	dd (°N)	u_{10} (m s^{-1})	H_s	τ_p (s)	z_s (m)
III	3 Dec 1993	NE Pacific 48°57′N, 127°00′W	80	320 $\sigma = 8$	Increasing, 11–16 $\sigma = 1.4$	Growing, 4–4.8	Increasing, 9–10	0.18
IV	9 Dec 1993	NE Pacific 48°57′N, 127°00′W	Unlimited	120–180 $\sigma = 7$	Increasing, 12–20 $\sigma = 1.9$	Growing, 4–6.6	Increasing, 8–12	0.19
V	18 Apr 1995	NE Pacific 36°15′N, 122°26′W	Unlimited	325 $\sigma = 15$	Increasing, 10–14 $\sigma = 1.6$	Growing, 3–3.8	Increasing, 6–7 swell: 11.5	0.12

breaking process. The strong role of wave groups in the breaking process at sea is highlighted in the observational literature in the papers by Donelan et al. (1972) and more recently Holthuijsen and Herbers (1986). The recent paper by Donelan et al. (1996) provides a succinct overview of the observational and theoretical literature on a quasi-two-dimensional wave packet representation for ocean waves and describes a directional wavelet approach for analyzing directional wave group behavior in directional wave measurements.

The extensive observational background and current status of wave breaking probability for the wind-driven sea surface is reviewed comprehensively in recent papers by Gemmrich and Farmer (1999, hereafter GF) and Banner et al. (2000, hereafter BBY). Motivated by a perceived strong dependence of breaking onset on nonlinear wave group hydrodynamics and the apparent lack of any strong underlying correlation with wind speed or wave age, BBY proposed a threshold variable for the wave breaking probability of the dominant wind waves based on the *mean* steepness of these waves. The dominant wind waves are defined as those with frequencies within $\pm 30\%$ of the spectral peak frequency f_p, with the dominant wave period taken as f_p^{-1} and associated with each individual dominant wave is a dominant wave crest. The breaking probability was defined as the ratio of dominant breaking wave crests to total dominant wave crests passing a fixed point during a given time interval. Also, BBY used the significant steepness $\varepsilon = H_p k_p/2$ as a convenient measure of the mean nonlinearity of the dominant waves, where H_p is the significant height based on integrating the wave height variance spectrum over a bandwidth embracing the dominant waves. Field datasets processed on this basis showed a robust correlation for a very wide range of wind and wave conditions. While there was considerable scatter, this correlation indicated a clear threshold behavior, with negligible breaking for $\varepsilon < \varepsilon_T$, the threshold significant steepness, and an approximately quadratic behavior on $(\varepsilon - \varepsilon_T)$ when $\varepsilon > \varepsilon_T$. BBY also included a very preliminary analysis of whether a breaking threshold based on mean steepness was operative for waves shorter than the dominant windseas. They found that this viewpoint was not inconsistent with the very limited dataset available to them, even with the very considerable scatter.

In the present paper, we report results of our further analysis of the extensive open ocean datasets described by GF. From their study, GF concluded that the overall breaking probability for all scales of whitecapping breaking waves did not correlate well with traditionally adopted measures such as the wind speed or spectral peak wave age. Similar conclusions were also reported by BBY. Among the major findings reported in GF were a strong correlation of overall breaking probability with wind input relative to the wind input for fully developed windsea conditions, with the median value of the period of breaking waves approximately one-half of the dominant wave period. They also reported that the typical height of breaking waves was about 70% of the significant wave height, which implies extremely steep waves for this spectral subrange. However, we now believe that this conclusion was biased by the crest-counting method used by GF. This bias has been removed in the crest-counting algorithm used in the present investigation.

The availability of the GF dataset presented a unique opportunity to undertake a detailed analysis focusing on the validity of a mean steepness-based breaking threshold criterion for wave scales both at the spectral peak and in spectral subranges up to 2.5 times the spectral peak frequency.

2. The measurements

Full details of the instrumentation, deployments, measurement techniques (including breaker detection), and logistical difficulties, together with meteorological and oceanic conditions for the gathered datasets, are given in sections 2 and 3 of GF and the reader is referred to that paper.

For the present analysis, only the deployments III, IV, and V were considered suitable since deployments I and II did not include surface elevation data at the location of the conductivity sensors and therefore do not provide information on the size of the breaking waves for those datasets. Table 1, extracted from GF, sum-

marizes the conditions of the three deployments analyzed in the present study.

3. Data analysis methodology

a. Definition and estimation of breaking probability

Breaking probability is traditionally defined as the ratio of the passage rates of breaking crests to total number of wave crests past a fixed point for a statistically robust sample size, regardless of wave scales involved. To be able to differentiate wave scale in the framework of breaking probability, we refine this definition of breaking probability by extending the framework introduced by Phillips (1985, section 6).

If $\Lambda(\mathbf{c})$ is the spectral density of breaking wave crest length per unit area with velocities in the range ($\mathbf{c}$, $\mathbf{c} + d\mathbf{c}$), then the passage rate of breaking crests in ($\mathbf{c}$, $\mathbf{c} + d\mathbf{c}$) past a fixed point is $c\Lambda(\mathbf{c})d\mathbf{c}$. We need to introduce the analogous concept of the spectral density of the total wave crest length per unit area $\Pi(\mathbf{c})$ such that the *total* crest passage rate in ($\mathbf{c}$, $\mathbf{c} + d\mathbf{c}$) past a fixed point is $c\Pi(\mathbf{c})d\mathbf{c}$. The breaking probability for wave scales $\mathbf{c}$ is then defined as

$$P(\mathbf{c}) = \frac{\int c\Lambda(\mathbf{c})\, d\mathbf{c}}{\int c\Pi(\mathbf{c})\, d\mathbf{c}}.$$

Analogous definitions can be formulated for azimuth-integrated forms of P with scalar independent variables c (phase speed), k (wavenumber magnitude), or f (frequency).

We note that it is essential that the same scale bandwidth must be used in the numerator and denominator when determining the breaking probability from observations. While this is assumed implicitly when overall breaking probabilities are estimated, we have adhered closely to this requirement in our determination of breaking probability for waves of different scales. For the present dataset, these were based on wave period bands or their equivalent frequency bands. Although the choice is arbitrary, we used two frequency spectral bandwidths in our analysis to verify that the results were insensitive to the bandwidth. These were *relative* frequency bandwidths about the center frequency f_c of $\pm\delta f_c$, with $\delta = 0.15$ and 0.30, where the latter corresponds to the spectral peak bandwidth adopted in BBY. The use of a constant relative frequency bandwidth maintains a consistent relative wave period or wavelength bandwidth for different wave scales. We verified that using a constant bandwidth $\pm\delta f_p$ about f_c produced very similar results.

The determination of breaking probabilities requires counting the number of breaking crests and total wave crests occurring in a given scale bandwidth over a statistically significant sampling interval. The traditional method of counting wave crests is based on zero-crossings of the wave height signal (e.g., see Holthuijsen and Herbers 1986). While this is useful for the dominant sea waves, it misses many of the ''riding waves,'' which are defined as the shorter waves that are identified on the longer dominant waves through their local short period signature in the wave height record. The following section describes the methodology that was used in this study to estimate these statistics, including the procedure for assigning each detected wave crest and breaking event systematically to an appropriate spectral band. The results for the spectral breaking probabilities and associated statistics are described subsequently.

b. Methodology

Counting the passage rate of individual wave crests of short waves riding on longer waves from a single-point wave height record is a time-honored but challenging task. We examined a number of decomposition methods for this problem—for example, Fourier bandpass filtering, wavelet analysis, and a novel method known as the empirical mode decomposition introduced recently by Huang et al. (1998). However, after investigating these techniques in detail, we found that they either introduced spurious riding waves, were unable to reliably localize and quantify the riding waves, or needed an associated bandwidth, contrary to a basic premise of the breaking probability definition given above. With these reservations on their reliability for our application, we devised and implemented the crest-counting technique described below. We believe this approach makes far fewer assumptions and leads to fewer spurious crest registrations in the process of identifying and quantifying the passage rates of different scales of wave crests, both nonbreaking and breaking, passing our measurement location.

c. Riding wave removal (RWR) method

We adapted the traditional zero-crossing approach to determine the properties of shorter riding waves in addition to the dominant wind waves. Our starting point was the method described in section 4 of GF, which detected zero-crossings of the derivative of the elevation signal to register the shorter riding waves. Because of the signal-to-noise ratio, only waves with elevation differences exceeding 0.1 m between trough and crest and between crest and following trough were counted as individual waves. We note also that in GF, a scale decomposition of the breakers was not required, just a total count. However, in the present context, we observed that the GF partitioning algorithm had a tendency to alias longer waves to higher frequencies when a short wave is detected riding on the longer wave. We developed a variation on this method designated the ''riding wave removal'' (henceforth RWR) method that pro-

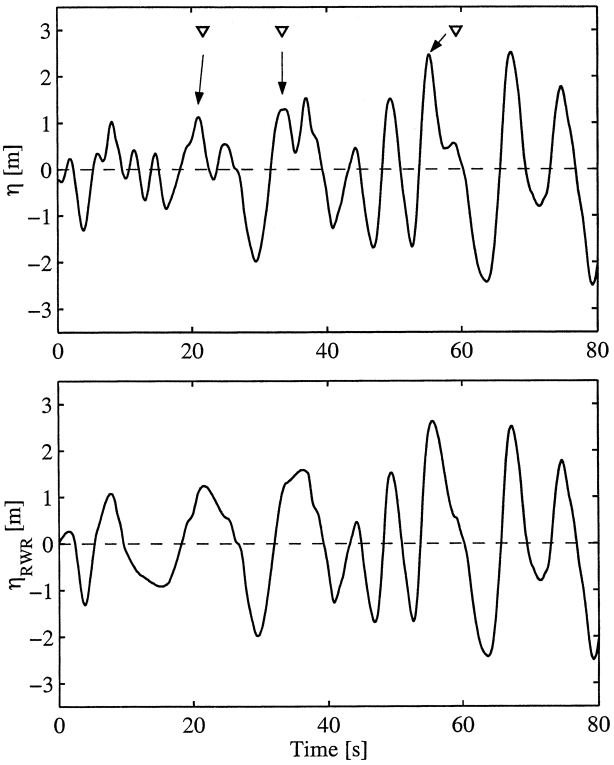

FIG. 1. Plot of 80-s elevation time series showing the riding wave extraction and replacement according to the RWR decomposition method. In the upper panel, the detected breaking events are indicated by the triangles, with the corresponding breaking crests identified by the breaker association algorithm indicated by the arrows.

gressively detects and then removes riding waves through an iterative automated processing.

The first phase of the analysis determined the set of upward zero-crossing intervals in the time derivative of the wave height record and these were sorted by period. The shortest-period oscillation identified the shortest riding wave. Its measured characteristics (period, crest-to-trough height, and location in the time series) were stored in a file and this wave was then removed from the elevation series by replacing it with a least squares fit cubic polynomial spliced to suitable end points on the underlying longer wave form. The analysis was then repeated on the modified wave height record making sure that no new riding waves were created and then counted by the removal/smoothing methodology. The minimum elevation difference requirement of 0.1 m associated with signal-to-noise considerations mentioned above was retained in this analysis. This process was iterated until the period of the riding wave extracted was about 0.55 of the dominant wave period or, equivalently, a frequency of 1.9 times the spectral peak frequency f_p. This choice of period for terminating the extraction of riding waves was found to maximize the number of dominant waves detected subsequently in the chosen spectral peak frequency band of f_p $(1 \pm \delta)$, with $\delta = 0.3$. Figure 1 demonstrates a typical application of this method applied to a typical 80-s record. Further details of this procedure are given in appendix A. This set of waves provides the collective data set identified as the ''detected'' crests. These identified crests are to be distinguished from the set of ''nominal'' (potentially nonphysical) crests that result from a Fourier band-pass filtering applied to the wave height signal. In the present context, these nominal crests are useful only as a notional reference.

Our analysis then sought to determine the individual wave to which each breaking event detected by the air-void sensor belonged. It calculated this association algorithmically on the basis of minimizing the relative lag between the time of the breaking event and the time of the nearest detected crest, while also satisfying a local steepness threshold $ak > 0.075$, based on the wave height and period extracted from the RWR analysis. Here a is the local wave amplitude, defined as one-half of the mean crest-to-trough height of the forward and trailing face, and k is the local wavenumber, calculated from the wave period using the linear dispersion relation for deep water gravity waves. Each detected breaking event was assigned to the individual wave with the minimum relative phase lag: if two waves had near-identical relative phase lags, the algorithm assigned the breaker to the steeper wave. In this way, a corresponding file was compiled of the detected breakers with their occurrence time, frequency and steepness, as defined above in this paragraph. Figure 2 gives a graphical summary of the relevant statistics obtained from the RWR decomposition analysis of experiment IV. These statistics include the probability distributions of wave period and wave steepness for all waves and for all detected breaking events (Figs. 2a,b). The median breaking wave period is $\tau_{\text{med}} = 6.9$ s. The distribution of time lead or lag of each detected breaking event normalized with respect to the period of its parent (associated) wave crest is divided into two subsets (Fig. 2c), corresponding to (i) shorter waves ($\tau < \tau_{\text{med}}$) and (ii) longer waves ($\tau \geq \tau_{\text{med}}$). We allowed the normalized time lag $d\tau_{\text{RWR}}$ between the breaker and crest registrations to range from -0.25 to $+0.75$ to allow for a range of possible breaking detection scenarios. At one extreme, corresponding to $d\tau_{\text{RWR}} < 0$, the leading edge of a well-developed spilling breaker is registered in advance of the broken wave crest, while at the other extreme, the passage of an incipiently breaking crest is registered and there is a significant delay in the time for the diffusing bubble plume to be advected back to the air void sensor by the rearward orbital motion of the associated wave trough. Absolute time lags <2 s are considered to be within the bubble injection time and for events within this short absolute time lag, no restriction on the relative time lag has been imposed. The specified bounds for $d\tau_{\text{RWR}}$ allow for additional uncertainty due to possible asymmetry in the shape of the forward and rear faces of the waveform. Further, we considered that events with an absolute time lag greater than 5 s, corresponding to less than 5% of

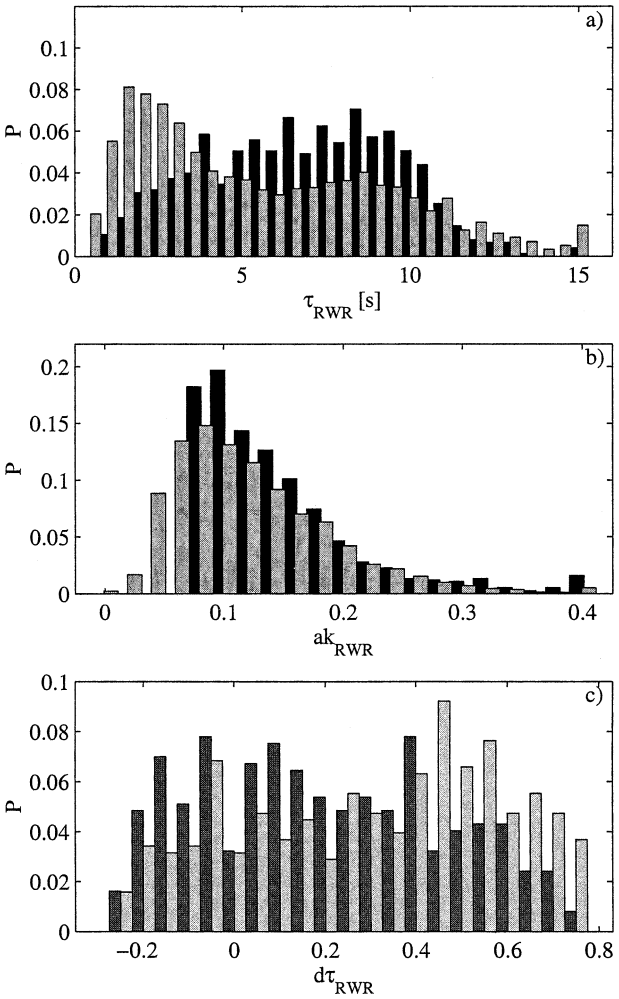

FIG. 2. Overall statistics from the RWR and breaking event analyses of run IV, according to the definitions given in section 3: (a) probability distributions P of wave period τ and (b) probability distributions P of the wave steepness ak_{RWR}. Light gray bars correspond to all waves, black bars to the breaking waves. (c) Probability distributions P of $d\tau_{\mathrm{RWR}}$ the time lead $(-)$ or lag $(+)$, normalized by wave period, of the detected breaking event with respect to its parent (associated) wave crest. Light gray bars correspond to shorter waves with period $\tau < \tau_{\mathrm{md}}$, dark gray bars to longer waves with $\tau > \tau_{\mathrm{md}}$, where τ_{md} is the median breaking wave period.

the total detected breaking events, probably do not represent active breakers and, therefore, these were rejected. Changing the restriction of the absolute time lag within reasonable bounds altered the breaker association only marginally. In total, up to $O(30\%)$ of breaking events could not be associated with a parent wave crest and these events are not included in the subsequent analysis. However, it was reassuring to note that when these bounds were modified, while the fraction of breakers that could be classified may have changed, the basic distributions of breaking probability f_{RWR} with respect to the saturation σ were insensitive to these changes.

As discussed in detail in section 3, the crest passage rate in any given spectral band including the dominant wave subrange (spectral peak subrange) determined by the RWR method depends strongly on the relative spectral bandwidth δ and is significantly less than the nominal center frequency of that band for our choices of δ. However, since the same bandwidth is used in the numerator and denominator to determine the breaking probability, the dependence on δ is not critical in estimating robust spectral breaking probabilities.

4. Results

Before presenting the detailed spectral results, we note that an initial check was carried out on how well the GF data agreed with the correlation curve in BBY for the dominant wave breaking probability. We calculated the significant steepness parameter ε of the wind sea spectral peak band for each 30-min record in each of the deployments, based on the definition for ε used in BBY:

$$\varepsilon = \frac{H_p k_p}{2},$$

where

$$H_p = 4\left[\int_{0.7\,f_p}^{1.3\,f_p} F(f)\,df\right]^{1/2}$$

and $F(f)$ is the frequency spectrum of the windsea. The dominant wave breaking probability data for the GF data were found to closely overlie the BBY data trend. This provided strong initial encouragement for the robustness of the breaking threshold on a mean wave steepness measure. However, being bandwidth sensitive, ε could not be easily generalized to other parts of the spectrum, motivating the present determination of breaking probability based on spectral steepness measures.

a. Crest count results

Using the RWR technique, systematic processing of the three data records (experiments III, IV, and V) yields the plots in Fig. 3. For the standard relative bandwidths $\delta = 0.15$ and 0.3, these results show the ratio of detected crests to the nominal crest count based on the nominal reference center frequency f_c for each spectral band. Based on our choice of a symmetric bandwidth, the RWR method produces a ratio of crest count to nominal crest count that decreases toward higher frequencies relative to the spectral peak. It is evident that significant differences exist between the crest count detected by the RWR method and the nominal reference center frequency f_c in any given spectral band including the spectral peak, where the ratio is around 0.7. The apparent ''shortfall'' at the spectral peak may arise from several sources. These include failure to count waves with small amplitudes that can occur at the transition between successive wave groups or phase-dependent superposition effects such as occur in coalescing chirped wave pack-

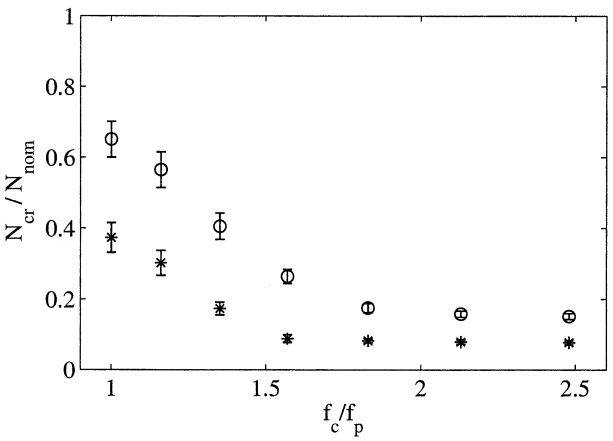

FIG. 3. Ratio of detected crest count N_{cr} to nominal crest count N_{nom} as a function of center frequency f_c relative to the spectral peak frequency f_p for the RWR analysis method used in this study. The range of center frequencies f_c/f_p was 1.0, 1.16, 1.35, 1.57, 1.83, 2.13, and 2.48. The open circles are for $\delta = 0.3$; the asterisks are for $\delta = 0.15$; and the error bars, representing one standard deviation, are shown superposed.

ets. Another possible source is our choice of a symmetric spectral bandwidth δ. The wave spectrum is noticeably asymmetric, and we found that increasing the upper bound of the bandwidth delivers a crest count closer to f_p. With the remote wave observation system deployed by GF, there is no further information available to independently validate the wave crest count, and this aspect should be addressed in future studies. In any event, for the present study, the breaking probabilities we estimate are insensitive to the choice of bandwidth.

b. Spectral steepness

The RWR crest counting method quantified the mean spectral wave steepness, as discussed in the methodology section above. Appendix B summarizes the breaking probabilities expressed in terms of the mean steepness of the ensemble of *breaking* waves identified by this method. Rather than seeking to relate breaking probability to the steepness of the subpopulation of breaking waves, we focused our investigation on validating a spectral measure of wave field nonlinearity as an appropriate independent variable. As a convenient nondimensional measure of spectral steepness, we chose the azimuthal-integrated spectral saturation

$$\sigma = \int_0^{2x} k^4 \Phi(k, \theta)\, d\theta,$$

where Φ is the wavenumber waveheight variance spectrum and $\mathbf{k}$ is the wavenumber vector. The spectral saturation density $B(\mathbf{k}) = k^4\Phi(\mathbf{k})$ was introduced by Phillips (1984) and it is easily shown using the linear gravity wave dispersion relation that the azimuth-integrated saturation σ has the equivalent form in terms of the frequency spectrum $F(\omega)$:

$$\sigma = \omega^5 F(\omega)/2g^2 = (2\pi)^4 f^5 F(f)/2g^2,$$

where ω is the radian frequency, $f = \omega/2\pi$, and g is the gravitational acceleration. We used observed values of σ as a primary bandwidth-independent measure of spectral steepness, as this quantity is available directly from measured single-point time series. The final correlations reported in this paper exploit the following close relationship between the local spectral saturation $k^4\Phi(\mathbf{k})$ and the mean square slope:

$$\text{mss} = \iint k^2 \Phi(k, \theta) k\, dk\, d\theta = \iint k^4 \Phi(k, \theta)\, d(\ln k)\, d\theta.$$

Hence the mss is easily calculated for any subregion in the directional spectrum by specifying the fractional bandwidth $d\ln(k) = dk/k = 2df/f$ and angular spreading bandwidth $d\theta$ about the mean wave direction.

The corresponding breaking probabilities were calculated for a range of center frequencies f_c above the spectral peak frequency for the two standard spectral relative bandwidths $\delta = 0.15$ and 0.3. We verified that the breaking probability was insensitive to the analysis bandwidth δ. This range of center frequency bands and relative bandwidths provides a less sparse indication of the trend of breaking probability with f_c/f_p than if calculated over nonoverlapping bands and demonstrates the robustness of the results. The results for the GF datasets III, IV, and V for the spectral peak and higher frequency bands are shown in Fig. 4.

This plot shows clearly that a saturation threshold is operative in each of the frequency bands and this is the major result of this paper. However, it is seen that the threshold level of σ for breaking onset increases systematically with f_c/f_p and therefore does not provide a *common* breaking threshold for all frequency bands. In section 5, we advance a hypothesis that leads to a common breaking threshold.

c. Influence of the wave age of the dominant seas

Deployment IV on 9 December 1993 provided an opportunity to monitor the evolution of the breaking probability over a ten hour period, during which the spectral peak wave age $c_p/u_{\lambda/2}$ increased appreciably. The scaling wind speed $u_{\lambda/2}$ was taken as the mean wind at a height of one half of the dominant wavelength. The other two deployments had much lower wave age variations. For each of the deployments, we examined the dependence of breaking probability on increasing wave age in the different f_c/f_p bands using the RWR method applied to 1-h data records. These results, shown in Fig. 5, do not reveal a strong correlation of breaking probability on the spectral peak wave age in any of the spectral subranges, nor is there evidence of threshold behavior.

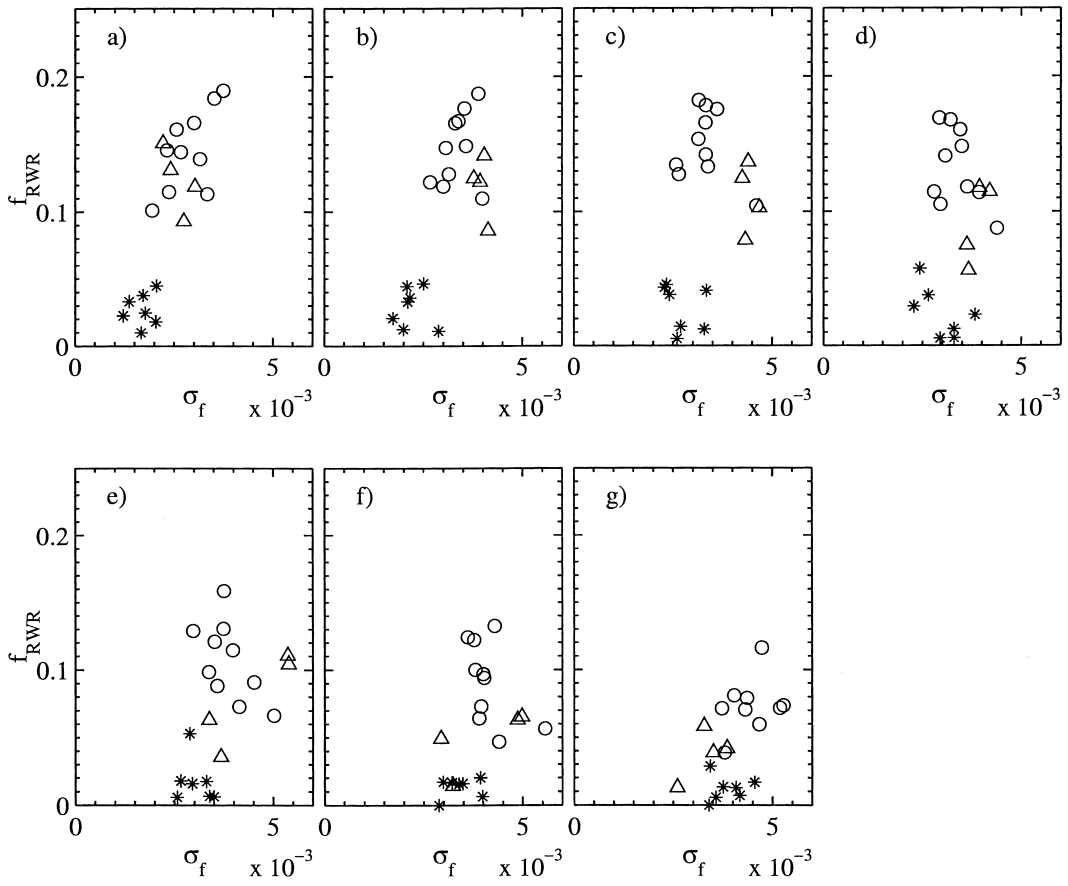

FIG. 4. Breaking probability f_{RWR} based on the riding wave decomposition method against σ, the azimuth-integrated saturation for the range of center frequencies f_c/f_p investigated in this study: (a) $f_c/f_p = 1.0$, (b) $f_c/f_p = 1.16$, (c) $f_c/f_p = 1.35$, (d) $f_c/f_p = 1.57$, (e) $f_c/f_p = 1.83$, (f) $f_c/f_p = 2.13$, and (g) $f_c/f_p = 2.48$. The symbols *, ○, and Δ represent, respectively, the deployments III, IV, and V described in Table 1.

However, despite the considerable scatter, it is interesting to note that the breaking probability of the spectral peak waves remained more or less constant with wave age, while breaking probabilities of the higher frequency components tended to increase as the wind sea aged. Thus, for the wave ages observed in the GF deployments, the dominant seas were still sufficiently steep that we were not able to observe the expected decrease of breaking probability to zero for very old windseas.

5. Discussion and conclusions

In this study, we conducted a detailed examination of breaking probability for a range of wave scales based on relating the passage rate of individual breaking crests to the passage rate of individual wave crests in the same scale bandwidth. Our primary result demonstrated a clear threshold dependence of breaking probability on the wave spectral saturation in each of the frequency ranges examined. This finding provides strong support for the proposition that a hydrodynamic threshold variable is operative for the breaking probability of gravity waves both at and above the spectral peak of the windsea.

In the vicinity of the spectral peak, the present results also reinforce the strong correlation with significant wave steepness of the diverse datasets reported recently by BBY for dominant breaking waves. In particular, the near-linear dependence of breaking probability on σ parallels the near-quadratic dependence on significant peak steepness reported by BBY. However, the significant wave steepness parameter used by BBY is not readily transferred to higher frequency bands above the spectral peak because of its intrinsic bandwidth requirement, among other reasons. Accordingly, our study focused on the dependence of breaking on the azimuth-integrated spectral saturation σ, which provides a measure of spectral steepness independent of spectral bandwidth.

From the results in Fig. 4, we noted that as the center frequency f_c increases above f_p, the spectral saturation σ provides a clear threshold for breaking for all frequencies observed. The breaking threshold value of σ is seen to nearly double over the directionally expanding spectral subrange $1 < f_c/f_p < 2.48$ investigated in this study. However, the structural similarity of the robust

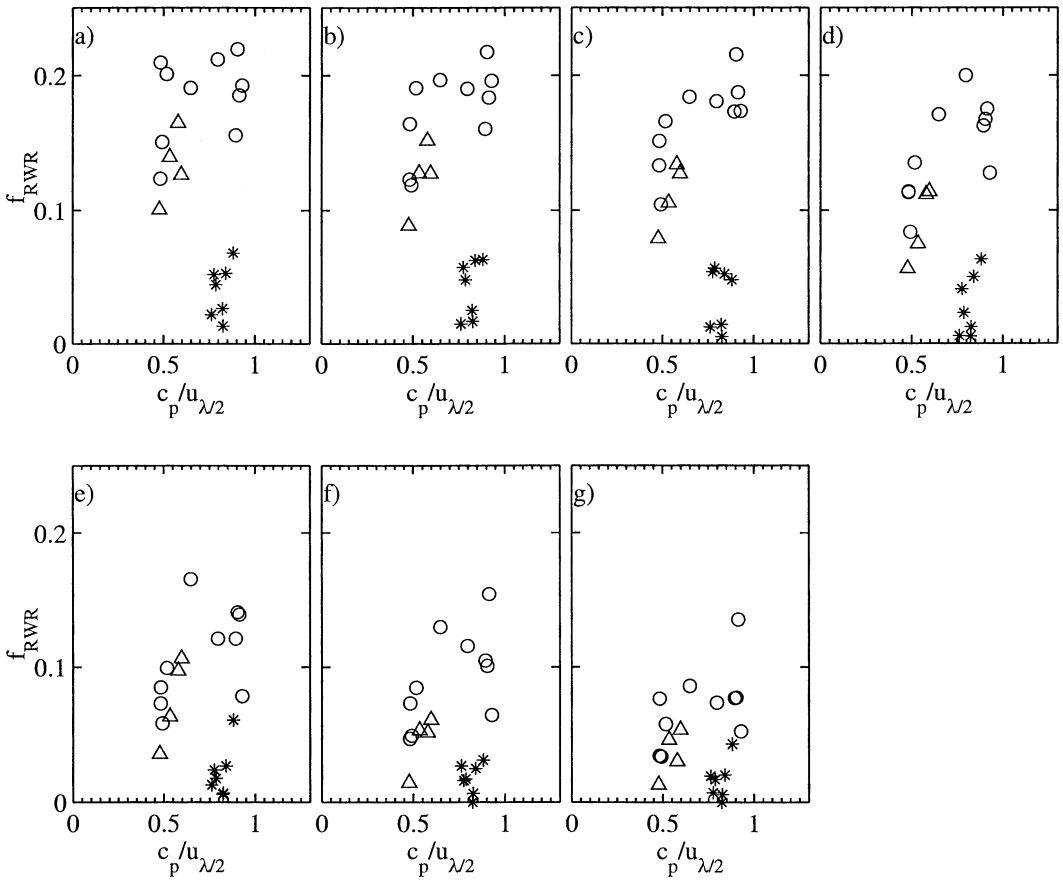

FIG. 5. Breaking probability f_{RWR} estimated by the RWR method against spectral peak wave age $c_p/u(\lambda_p/2)$ for the range of center frequencies f_c/f_p investigated in this study: (a) $f_c/f_p = 1.0$, (b) $f_c/f_p = 1.16$, (c) $f_c/f_p = 1.35$, (d) $f_c/f_p = 1.57$, (e) $f_c/f_p = 1.83$, (f) $f_c/f_p = 2.13$, and (g) $f_c/f_p = 2.48$. Symbols are as in Fig. 4.

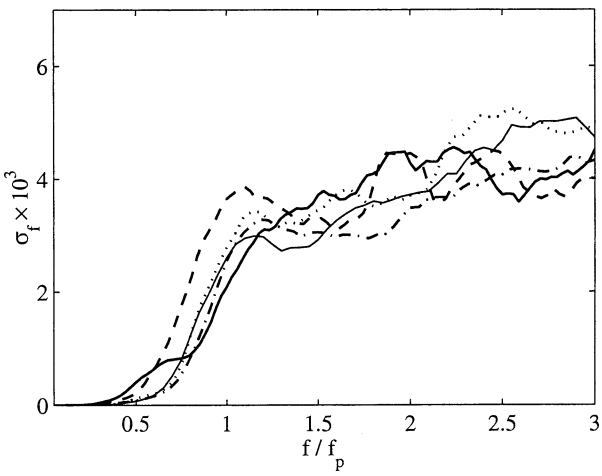

FIG. 6. Evolution of azimuth-integrated spectral saturation (σ) against frequency normalized by dominant frequency for experiment IV. Data are shown at 2-h intervals with corresponding line styles thick solid, dash, dash–dot, dot, thin solid, respectively.

threshold behavior seen in the different spectral bands is very suggestive of a universal behavior, which is explored below.

It is well known (e.g., Banner 1990) that above the spectral peak, the directional spreading of the windsea broadens. Based on the quasi-two-dimensional nonlinear wave group viewpoint foreshadowed in the introduction, we decided to remove the effect of different spreading widths for each f_c by normalizing σ by the *local* angular spreading width $\theta(f_c)$ of the directional wave spectrum. This gives the normalized saturation per unit spreading angle,

$$\tilde{\sigma}(f_c) = \sigma/\theta(f_c). \tag{5.1}$$

To implement this normalization, we used equation (19a) in Hwang et al. (2000), which provides an empirical relationship for the frequency-dependent directional spreading angle $\theta(f_c)$ at and above the spectral peak that agrees closely with their highly spatially sampled scanning laser altimeter data, and also with the empirical relationship proposed by Banner (1990). The results of Hwang et al. show that the angular spreading width nearly doubles over our investigated frequency range.

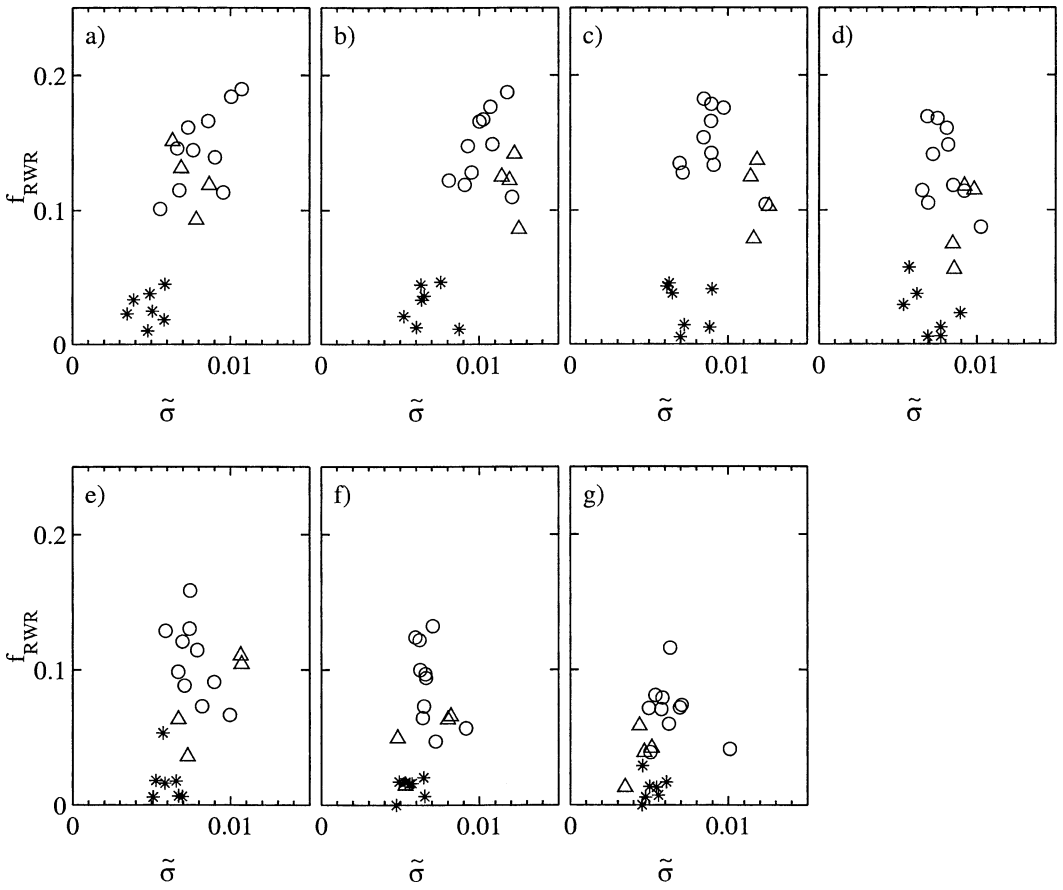

FIG. 7. Breaking probability f_{RWR} based on the RWR decomposition method against $\tilde{\sigma}$, the azimuth-integrated saturation normalized by the local spectral spreading width $\theta(f_c)$ defined by Eq. (5.1), for the range of center frequencies f_c/f_p investigated in this study: (a) $f_c/f_p = 1.0$, (b) $f_c/f_p = 1.16$, (c) $f_c/f_p = 1.35$, (d) $f_c/f_p = 1.57$, (e) $f_c/f_p = 1.83$, (f) $f_c/f_p = 2.13$, and (g) $f_c/f_p = 2.48$. The symbols are as in Fig. 4.

Figure 6 shows the typical observed variation of the azimuth-integrated spectral saturation σ with f_c/f_p during one of the observation periods (expt IV), from which it is evident that σ increases with f_c/f_p. Normalizing σ by the spectral spreading width $\theta_p(f_c)$ compensates for the increasing angular spreading with f_c/f_p, thereby reducing the increase in spectral saturation for $f_c > f_p$ due to the increasing directional spreading. The results for the breaking probability expressed in terms of the normalized saturation $\tilde{\sigma}(f_c)$ defined in (5.1) are shown in Fig. 7.

As seen in Fig. 7, it is evident that this approach provides a *common* saturation threshold for breaking of $\tilde{\sigma} \sim 4.5 \times 10^{-3}$ applicable over the energetic wave spectral subrange $1 < f_c/f_p < 2.48$ investigated in this study. We note that the strong increase in directional spreading in this spectral subrange might be expected to result in enhanced wave breaking probability associated with crossing directional components, but this does not show up in the observations. Instead, the collapse of the results in different frequency bands suggests that breaking ocean waves may be associated with predominantly quasi-two-dimensional wave group energetics, as described in Song and Banner (2002), among others.

Further investigation of the validity of this viewpoint is left to future observational studies that extend to shorter wave scales and are capable of providing simultaneous directional spectral resolution of the wave field and associated breaking events. Directionally resolved breaking data of this kind will provide deeper insight into the fundamental properties of wave breaking at sea and should allow a more refined parameterization of the breaking probability and associated dissipation rates that are central to improved spectral wind wave modeling.

We noted that the breaking probabilities when expressed in terms of the mean steepness of the ensemble of *breaking* waves also appears consistent with a threshold behavior. However, in view of their peripheral interest in the context of the underlying nonlinear hydrodynamical framework proposed for breaking onset, these results are included for reference in appendix B.

It is also of interest to discuss briefly how the present

results relate to previous findings of GF. In their Fig. 2, GF report their finding that the probability distribution of breaking waves has its maximum for waves with periods about one-half of the spectral peak period, in general agreement with the earlier findings of Melville (1994) and Ding and Farmer (1994). The present results provide a complementary perspective, expressing the relative probabilities of breaking in spectral bands in terms of an underlying hydrodynamical variable that reflects the mean nonlinearity of the waves in those spectral bands.

Last, we note that while significant whitecaps certainly can occur in isolation, they are commonly observed in association with well-defined dominant wave groups. Following such an evolving wave group, these whitecaps often occur successively at the steepest crests that periodically occur at the maximum of the wave group envelope, as reported in Donelan et al. (1972) and Holthuijsen and Herbers (1986), among others. Our study has not focused explicitly on these fundamental structural details and this aspect warrants further investigation through future studies involving spatially extensive datasets.

Acknowledgments. MLB gratefully acknowledges the support of the Australian Research Council and the U.S. Office of Naval Research for supporting his air–sea interaction research. ONR Grant N00014-93-1-0469 facilitated the participation of JRG and DMF in this collaboration. We also acknowledge the programming assistance of Eric Schulz in extending the RWR method. MLB also acknowledges stimulating discussions with Tony Elfouhaily.

APPENDIX A

Further Details on the RWR Decomposition Method

This appendix provides further details on the RWR methodology used in this study to extract wave crest passage rates from an elevation time series measured at a fixed location. The discussion is illustrated by the results of analyzing a typical data record of length 400 s taken halfway through deployment IV.

This method first calculated the peak frequency from the spectrum. It then analyzed the derivative of the wave height signal for zero-crossings, identifying the height, period, and phase of each riding wave. The RWR process starts by removing the shortest period riding wave and replacing it using the Matlab routine ''polyfit'' by a smooth curve (up to third-degree polynomial) spanning the removed subinterval between suitable endpoints. These end points were taken as the locations of the previous and following slope extrema, depending on whether the riding wave was detected at a longer wave crest, trough, forward face, or rear face. The interpolating polynomial curve was fitted to three successive points at each end of this subinterval to ensure a close match of end derivatives. Considerable care was taken to ensure that the interpolated curve did not significantly distort the steepness of the underlying larger scale wave nor create slope discontinuities that might be detected subsequently as spurious riding waves. This process was repeated iteratively, progressively removing lower frequency riding waves until it was terminated at a cutoff frequency determined empirically as $1.9 f_p$, which was found to maximize the number of wave crests in the dominant wave band, determined by a standard zero-crossing analysis of the RWR-transformed wave height time series. This is visualized in Fig. A1, which shows typical results for the RWR decomposition: the original wave height time series, this signal after RWR processing, and the typical sensitivity of the detected dominant wave crest count to the RWR cutoff frequency.

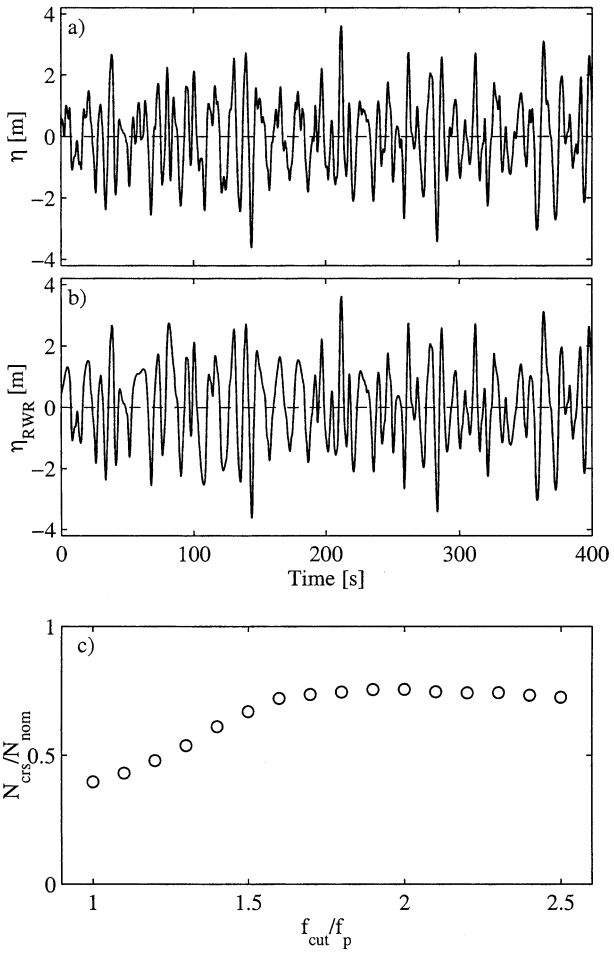

FIG. A1. (a) Four-hundred-second segment of the time series of surface elevation from deployment IV. (b) The resultant elevation record after riding wave removal (RWR) decomposition terminating at $1.9 f_p$. (c) Number of dominant wave crests detected as a function of the choice of terminating frequency f_{cut} above the spectral peak frequency f_p.

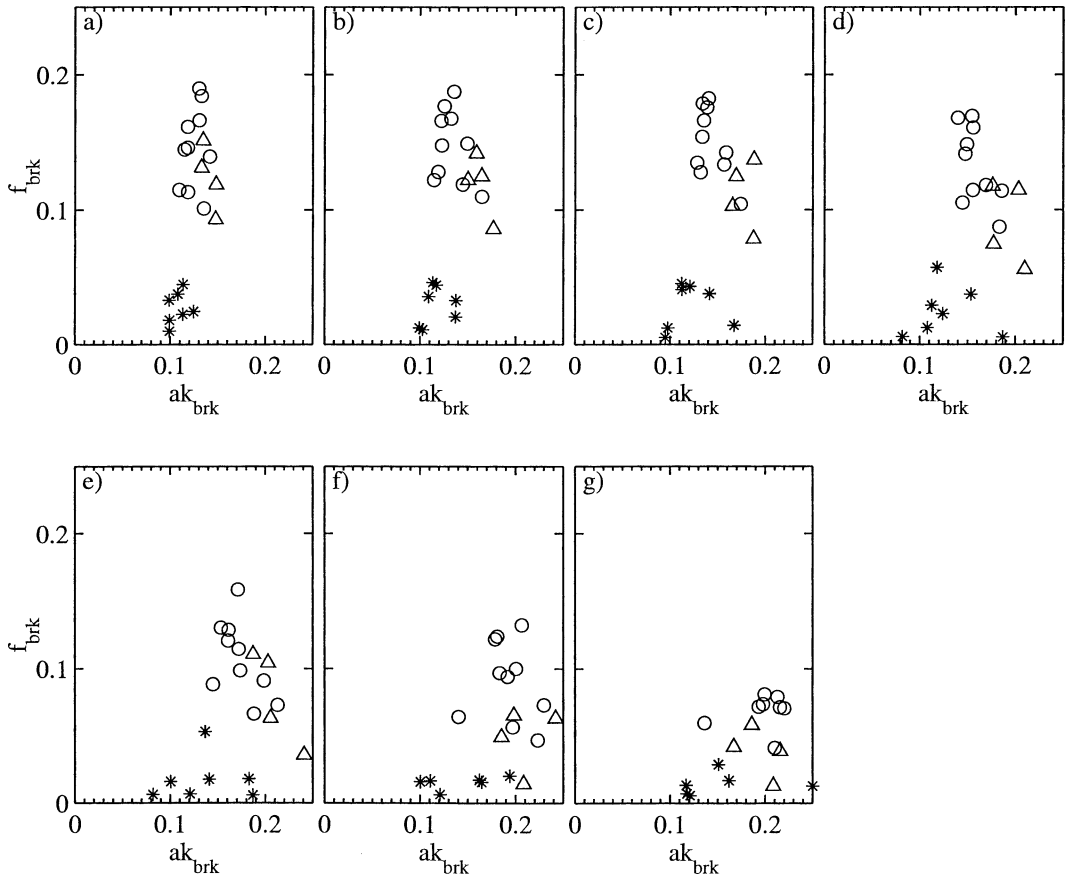

FIG. B1. Breaking probability against mean steepness ak_{BRK} of the RWR-detected breaking waves in the prescribed bandwidth δ for the range of center frequencies f_c/f_p investigated in this study: (a) $f_c/f_p = 1.0$, (b) $f_c/f_p = 1.16$, (c) $f_c/f_p = 1.35$, (d) $f_c/f_p = 1.57$, (e) $f_c/f_p = 1.83$, (f) $f_c/f_p = 2.13$, and (g) $f_c/f_p = 2.48$. The symbols are as in Fig. 4.

APPENDIX B

Dependence of the Breaking Probability on the Mean Steepness of the Breaking Waves

The central theme of this paper has been to investigate whether a measure of nonlinearity defined in terms of a spectral measure of wave steepness can provide a robust threshold variable for correlating breaking probability of wave scales considerably above the spectral peak. It is also of interest to examine whether this threshold behavior can be observed in terms of the ensemble mean of the steepness levels of individual breaking waves within the decomposition bands.

Figure B1 presents plots of observed breaking probability against the corresponding observed ensemble mean of individual breaking wave steepness determined from the RWR analysis output. In these figures, the results were constructed using frequency bins with the center frequencies of $f_c/f_p = 1.0$, 1.16, 1,5, 1.57, 1.83, 2.13, and 2.48 and a relative frequency bandwidth $\delta = 0.3$. Based on the ensemble average of individual breaking wave steepness levels, the results shown in these figures generally support the threshold behavior found using the spectral steepness measures. The results in Fig. B1 show clear threshold behavior near the spectral peak, but the scatter becomes very appreciable in the higher frequency bands. While of interest, the details of these correlations with the statistics of steepness of individual breaking waves are peripheral to the main results of this paper and will not be pursued further here.

REFERENCES

Banner, M. L., 1990: Equilibrium spectra of wind waves. *J. Phys. Oceanogr.,* **20,** 966–984.

——, and D. H. Peregrine, 1993: Wave breaking in deep water. *Annu. Rev. Fluid Mech.,* **25,** 373–397.

——, and X. Tian, 1998: Determining the onset of wave breaking for modulating surface gravity water waves. *J. Fluid Mech.,* **77,** 2953–2956.

——, and J.-B. Song, 2002: On determining the onset and strength of breaking for deep water waves. Part II: Influence of wind forcing and surface shear. *J. Phys. Oceanogr.,* **32,** 2559–2570.

——, A. V. Babanin, and I. R. Young, 2000: Breaking probability for dominant waves on the sea surface. *J. Phys. Oceanogr.,* **30,** 3145–3160.

Ding, L., and D. M., Farmer, 1994: Observations of breaking wave statistics. *J. Phys. Oceanogr.,* **24,** 1368–1387.

Dold, J. W., and D. H. Peregrine, 1986: Water-wave modulations. *Proc. 20th Int. Conf. on Coastal Engineering,* Vol. 1, Taipei, Taiwan, ASCE, 163–175.

Donelan, M. A., M. S. Longuet-Higgins, and J. S. Turner, 1972: Whitecaps. *Nature,* **239,** 449–451.

——, W. M. Drennan, and A. K. Magnusson, 1996: Nonstationary analysis of the directional properties of propagating waves. *J. Phys. Oceanogr.,* **26,** 1901–1914.

Duncan, J. D., 2001: Spilling breakers. *Annu. Rev. Fluid Mech.,* **33,** 517–547.

Gemmrich, J. R., and D. M. Farmer, 1999: Observations of the scale and occurrence of breaking surface waves. *J. Phys. Oceanogr.,* **29,** 2595–2606.

Holthuijsen, L. H., and T. H. C. Herbers, 1986: Statistics of breaking waves observed as whitecaps in the open sea. *J. Phys. Oceanogr.,* **16,** 290–297.

Huang, N. E., Z. Shen, S. R. Long, M. C. Wu, Q. Zheng, N.-C. Yen, C. C. Tung, and H. H. Liu, 1998: The empirical mode decomposition and the Hilbert spectrum for nonlinear and non-stationary time series analysis. *Proc. Roy. Soc. London,* **454A,** 903–955.

Hwang, P. A., D. W. Wang, E. J. Walsh, W. B. Krabill, and R. W. Swift, 2000: Airborne measurements of the wavenumber spectra of ocean surface saves. Part II: Directional distribution. *J. Phys. Oceanogr.,* **30,** 2768–2787.

Melville, W. K., 1994: Energy dissipation by breaking waves. *J. Phys. Oceanogr.,* **24,** 2041–2049.

——, 1996: The role of surface-wave breaking in air–sea interaction. *Annu. Rev. Fluid Mech.,* **26,** 279–321.

Nepf, H. M., C. H. Wu, and E. S. Chan, 1998: A comparison of two- and three-dimensional wave breaking. *J. Phys. Oceanogr.,* **28,** 1496–1510.

Phillips, O. M., 1984: On the response of short ocean wave components at a fixed wavenumber to ocean current variations. *J. Phys. Oceanogr.,* **14,** 1425–1433.

——, 1985: Spectral and statistical properties of the equilibrium range in wind-generated gravity waves. *J. Fluid Mech.,* **156,** 505–531.

Rapp, R., and W. K. Melville, 1990: Laboratory measurements of deep water breaking waves. *Philos. Trans. Roy. Soc. London,* **331A,** 735–780.

She, K., C. A. Greated, and W. J. Easson, 1997: Experimental study of three-dimensional breaking kinematics. *Appl. Ocean Res.,* **19,** 329–343.

Song, J.-B., and M. L. Banner, 2002: On determining the onset and strength of breaking for deep water waves. Part I: Unforced irrotational wave groups. *J. Phys. Oceanogr.,* **32,** 2541–2558.

Thorpe, S. A., 1995: Dynamical processes of transfer at the sea surface. *Progress in Oceanography,* Vol. 35, Pergamon, 315–352.

Tulin, M. P., and J. Li, 1992: On the breaking of energetic waves. *Int. J. Offshore Polar Eng.,* **2,** 46–53.

——, and T. Waseda, 1999: Laboratory observations of wave group evolution, including breaking effects. *J. Fluid Mech.,* **378,** 197–232.

Waseda, T., and M. P. Tulin, 1999: Experimental study of the stability of deep-water wave trains including wind effects. *J. Fluid Mech.,* **401,** 55–84.